Biomechanical effects of maxillary expansion on a patient with cleft palate: A finite element analysis

Haofu Lee[a], **Alan Nguyen**[b], **Christine Hong**[a], **Paul Hoang**[c], **John Pham**[b], and **Kang Ting**[d]

Department of Orthodontics, School of Dentistry, University of California at Los Angeles, Los Angeles, Calif

Abstract

Introduction—The aims of this study were to evaluate the effects of rapid palatal expansion on the craniofacial skeleton of a patient with unilateral cleft lip and palate (UCLP) and to predict the points of force application for optimal expansion using a 3-dimensional finite element model.

Methods—A 3-dimensional finite element model of the craniofacial complex with UCLP was generated from spiral computed tomographic scans with imaging software (Mimics, version 13.1; Materialise, Leuven, Belgium). This model was imported into the finite element solver (version 12.0; ANSYS, Canonsburg, Pa) to evaluate transverse expansion forces from rapid palatal expansion. Finite element analysis was performed with transverse expansion to achieve 5 mm of anterolateral expansion of the collapsed minor segment to simulate correction of the anterior crossbite in a patient with UCLP.

Results—High-stress concentrations were observed at the body of the sphenoid, medial to the orbit, and at the inferior area of the zygomatic process of the maxilla. The craniofacial stress distribution was asymmetric, with higher stress levels on the cleft side. When forces were applied more anteriorly on the collapsed minor segment and more posteriorly on the major segment, there was greater expansion of the anterior region of the minor segment with minimal expansion of the major segment.

Conclusions—The transverse expansion forces from rapid palatal expansion are distributed to the 3 maxillary buttresses. Finite element analysis is an appropriate tool to study and predict the points of force application for better controlled expansion in patients with UCLP.

Cleft lip and palate (CLP) is the most common congenital defect involving the face and jaws; about 1 child in 700 children is born with the condition.[1] Embryologic studies show that failure of fusion between the medial and nasal processes with the maxillary processes leads to clefting of the lip and palate.[2] The cleft disrupts the structural integrity of the palate and results in mediolingual rotation of the minor segment of the maxilla. The collapsed minor segment is a common clinical feature in patients with unilateral CLP (UCLP) and is

Address correspondence to: Kang Ting, Orthodontics, UCLA School of Dentistry, 10833 Le Conte Ave, CHS 30-117, Los Angeles, CA 90095; haofulee@ucla.edu.

[a]Assistant professor.
[b]Dental student.
[c]Orthodontic resident.
[d]Professor and chair.

thought to be due to the molding influence of the surrounding facial soft tissues.[3] It often results in a constricted palatal arch and severe anterior crossbite with or without a posterior crossbite that is isolated to the cleft side.[4]

Anterolateral expansion of the minor segment is required to correct the transverse discrepancy from the collapsed minor segment and to achieve an ideal arch form. Palatal expansion devices, such as the 4-banded quad-helix, fan-type expander, and slim-line expander, are used to achieve anterior expansion. However, anatomic differences that result from the cleft and the asymmetric nature of the crossbite in patients with UCLP often make more expansion necessary in the anterior than in the posterior palate. Typical palatal expansion devices, normally used for non-CLP patients, correct the maxillary deficiency by applying transverse orthopedic forces and expanding the palate in the molar region.[5] They do not target the problem area that is unique to patients with UCLP.

Rapid palatal expansion (RPE) is a common technique that is part of the comprehensive treatment for CLP patients,[5–8] since their limited transverse growth requires maxillary expansion.[8–10] Hence, maxillary expansion is routinely performed in CLP patients to coordinate the width discrepancies of the maxilla and the mandible.[8] Both clinical[3,6,11] and finite element model (FEM)[5,12] studies on CLP have shown an asymmetric response of the cleft and noncleft segments with expansion forces.[13] Analyses of non-CLP patients have shown that regardless of orthopedic forces placed on the intermaxillary sutures, the articulation between the maxilla and the pterygoid plate of the sphenoid bone is the limiting factor in the amount of expansion achieved.[13,14] Since the midpalate is missing and the maxillary bone is deformed in patients with CLP, the expansive forces from RPE and the resistance to expansion can be expected to be different than with non-CLP patients.[13] The maxillary expansion mechanisms of RPE in CLP patients can be better understood using the biomechanical stress-strain displacement response produced by the FEM.

Previous studies have not analyzed the stress distribution in the craniofacial complex of patients with UCLP based on the directions of optimum force necessary to obtain the required expansion in the anterior region of the minor segment without overexpansion of the posterior region. In this study, we aimed to create a 3-dimensional (3D) FEM of a patient with UCLP to investigate the stress distribution from RPE in the nasomaxillary complex and to determine the points of force application that achieve the desired expansion in the anterior and posterior maxilla to obtain an ideal arch form.

Furthermore, these results may be helpful in obtaining a more predictable clinical outcome for the distraction osteogenesis procedure in patients with UCLP.[15]

MATERIAL AND METHODS

Spiral computed tomography (CT) data originally for medical use were obtained from a 7-year-old girl with amniotic band syndrome and incomplete UCLP (0.300-mm layer; voxel size, $0.463 \times 0.463 \times 0.300$ mm^3). The volumetric data from the CT scan was imported using Mimics software (version 13.1; Materialise, Leuven, Belgium) to generate a 3D solid model of the patient's skull, and the midpalatal suture was incorporated to increase the

accuracy in this study (Figs 1 and 2). The hard and soft tissue volumetric data were stored in DICOM format with the relative radiodensity of the CT image represented in Hounsfield units. Threshold segmentation with settings of 238 and 3071 Hounsfield units was used to identify the hard tissues of interest, yielding a 3D mask of the entire skull.

The mask of the model was manually modified to remove the noise to create the complete cleft model needed for this study. Smoothing was performed 3 times on the surface of the mask with the built-in Laplacian function to remove sharp edges. Triangle reduction removed overlapping and redundant triangles that made up the mesh of the FEM. The 3D object was re-meshed to reduce the number of triangle elements to a minimum, but enough to still accurately represent the 3D model (Fig 2). The 3D mesh, the FEM of the skull, was imported into a general-purpose finite element analysis software (version 12.0; ANSYS, Canonsburg, Pa).

The material properties assigned to the elements were linear elastic and isotropic (Table I). Zero degree of freedom was imposed on the nodes along the foramen magnum (Fig 3).

Nine combinations of force application were considered to test all possible combinations of maxillary expansion using the deciduous molars, the permanent molars, or a combination of the molars as anchors (Table II). The 9 combinations were divided into 3 groups. Group 1 (Fig 4) had expansion forces applied transversely between the deciduous first and second molars, and the permanent first molars. Group 2 (Fig 5) consisted of 3 simulations with expansion forces applied anteriorly on the cleft side and posteriorly on the normal side. Group 3 (Fig 6) also consisted of 3 simulations with forces applied posteriorly on the cleft side and anteriorly on the normal side.

Palatal expansion was simulated by applying transverse expansion forces to the maxillary right deciduous first molars (URD) and second molars (URE) or the maxillary permanent first molars (U6) on both sides of the palate. Equal forces were applied between the teeth, and different force combinations were analyzed (Table II). Force levels between 700 and 1100 g were applied to achieve 5 mm of anterolateral expansion of the collapsed minor segment to stimulate correction of the anterior crossbite in a patient with UCLP. The transverse forces attempted to stimulate the resultant forces from either a jack-screw type of RPE expansion device placed directly between the teeth across the palate or a 4-banded quad-helix with more activation on the anterior region of the minor segment and minimal expansion of the posterior region. Upon completion of the simulation, first principal, third principal, and von Mises stresses resulting from the virtual RPE were measured.

RESULTS

The FEM generated from the spiral CT data contained 105,357 nodes and 371,605 elements. Element size was varied to keep the number of nodes and elements sufficiently low to maintain an accurate representation of the skull. Smaller elements were used in areas with high variations in the surface contour, such as the nasomaxillary and midpalatal suture regions. Larger elements were used in areas with flatter surfaces, such as the cranium.

When transverse forces were applied at the maxillary permanent molars (UR6-UL6) (Table II), the minor and major segments of the maxilla along the cleft site were separated, and the largest transverse displacement was produced at the cusp tips of the maxillary deciduous canines. The expansion of the minor and major segments resulted in a pyramidal opening on the side of the cleft with the base of the pyramid at the floor of the nasal cavity and the apex slightly above the frontonasal suture. For the occlusal aspect, the opening was wider in the anterior than in the posterior between the minor and major segments. The expansion was asymmetric, with greater displacement at the dentoalveolar region on the cleft side than on the normal side. Expansion caused lateral bending of the medial and lateral pterygoid plates of the sphenoid bone, and more displacement was observed at the inferior border of the pterygoid plates than at the superior. Minimal displacement was seen at the supraorbital and forehead regions.

In group 1, transverse expansion forces were applied between the following pairs of teeth: URD-ULD, URE-ULE, and UR6-UL6 (Table II). Stress levels on the cleft side were higher in all 3 models than on the normal side, and the highest stress was experienced when forces were applied across UR6-UL6 (Fig 7). The first principal stress distribution plot (Fig 4, *A*) of all 3 group 1 simulations showed high tensile stresses at the medial wall of the orbit slightly below the junction of the frontomaxillary suture, at the angle of the piriform aperture on the cleft side, and at the inferior rim of the orbit directly above the infraorbital foramen on the normal side. High stress levels were also seen on the inferoposterior area of the zygomatic process of the maxilla and the body of the sphenoid bones.

The third principal stress distribution plot showed high compression stress levels at the lingual surfaces of the teeth where forces were applied and at the interior area of the zygomatic process of the maxilla in all 3 models (Fig 4, *B*). Moderate to high levels of stress were experienced at the anterolateral rim of the orbits on the normal side, and only moderate stress was observed on the cleft side. Moderate stress levels extended anteriorly from the inferolateral angle of the orbit, superiorly to the frontozygomatic suture and posteriorly to the temporal fossa. There was mild stress in the floors and lateral walls of both orbits.

When transverse forces were applied across the lingual surfaces of URD-ULD, maximum displacement on the cleft side occurred at the incisal edge of the maxillary right deciduous canine (URC) and gradually decreased from the anterior to the posterior teeth with minimum expansion at the UR6. However, on the normal side, expansion was relatively level from the maxillary left deciduous central incisor (ULA) to the ULE when forces were applied to URD-ULD and URE-ULE, but there was a slight increase when forces were applied to UR6-UL6 and then a slight decrease at the UL6 for all 3 force applications.

In group 2, forces were directed anteriorly on the cleft side and posteriorly on the normal side, with expansion forces applied to the following pairs of teeth: URD-UL6, URE-UL6, and URD-ULE (Table II). First principal stress distribution plots (Fig 5, *A*) of all 3 models of group 2 showed high tensile stresses at the medial wall of the orbit slightly below the junction of the frontomaxillary suture and at the angle of the piriform aperture on the cleft side. High tensile stress was evident at the inferior rim of the orbit directly above the infraorbital foramen on the normal side. High levels of stress were experienced on the

inferoposterior area of the zygomatic process of the maxilla only on the cleft side when forces were applied to URD-UL6 and URE-UL6 but observed bilaterally when forces were applied to URD-ULE. In addition, the body of the sphenoid on the cleft side had increased stress levels. In all 3 expansion simulations, stresses were increased on the cleft side more than on the normal side (Fig 7).

The third principal stress distribution plots (Fig 5, *B*) of all 3 models demonstrated high compression stress levels at the lingual surfaces of the teeth where forces were applied, and at the inferior area of the zygomatic process of the maxilla on the cleft side. Mild to moderate stress levels were found at the lateral rims of both orbits, and high stress was seen at the body of the sphenoid on the cleft side (Fig 8).

Maximum displacement occurred on the cleft side at the incisal edge of the URC when transverse forces were applied anteriorly on the cleft side and posteriorly on the normal side, and there was a gradual decrease from the anterior to the posterior teeth, with minimum expansion at the UR6. The normal side showed relatively level expansion from the ULA to the UL6 for all 3 force applications. However, the amount of expansion varied, with minimal expansion when forces were applied to URD-UL6, moderate expansion when forces were applied to URE-UL6, and maximum expansion when forces were applied to URD-ULE. There was moderate expansion at the superior region of the alveolar bone and on the maxilla extending superiorly to the inferior region of the orbit bilaterally.

In group 3, forces were directed posteriorly on the cleft side and anteriorly on the normal side to the following pairs of teeth: UR6-ULD, UR6-ULE, and URE-ULD. The first principal stress distribution plots (Fig 6, *A*) showed high tensile stress at the medial wall of the orbit slightly below the junction of the fronto-maxillary suture of only the cleft side when forces were applied to UR6-ULE and URE-ULD. However, the high stress area extended mediosuperiorly along the fronto-nasalis suture when forces were applied to UR6-ULD. In addition, high stresses were detected at the angle of the piriform aperture on the cleft side and at the inferior rim of the orbit directly above the intraorbital foramen on the normal side. High stress levels were found at the body of the sphenoid, and stress areas were greater when forces were applied to UR6-ULD and UR6-ULE than when forces were applied to URE-ULD (Fig 7). There was greater stress on the hard palate on the normal side than on the cleft side, and it was highest when the area of force application was wide, particularly across UR6-ULD.

In all 3 models, third principal distribution plots (Fig 6, *B*) showed high compression stress levels at the lingual surfaces of the teeth and the inferior area of the zygomatic process of the maxilla. There was mild stress on the floors of both orbits and on the sphenoid bone at the base of pterygoid plates, but despite this, the area of stress was greater on the normal side than on the cleft side.

Maximum displacement on the cleft side occurred at the incisal edge of the URC and gradually decreased from the anterior to the posterior teeth, with minimum expansion at the UR6 when forces were applied to URE-ULD. Equal expansion of the cleft and normal sides

occurred when forces were applied to URE-ULD, but expansion on the normal side was greater than on the cleft side when forces were applied to UR6-ULE and UR6-ULD.

Summary of results

The craniofacial stress distribution was asymmetric, with higher stress levels on the cleft side. When forces were applied more anteriorly on the collapsed minor segment and more posteriorly on the major segment, there was greater expansion of the anterior region of the minor segment and minimal expansion of the major segment, which correlates to most patients with UCLP. Equal expansion of the cleft and normal sides occurred when forces were applied to URE-ULD. Expansion on the normal side was greater than on the cleft side when forces were applied to noncleft-side molars and cleft-side deciduous molars, UR6-ULE and UR6-ULD. The body of the sphenoid experienced the highest stress concentration from palatal expansion in all models. The first principal stresses at the body of the sphenoid bone on the cleft side are generally 1.5 times greater than those on the normal side. The third principal stresses at the body of the sphenoid bone on the cleft side are generally 2 times greater than those on the normal side.

DISCUSSION

The timing of expansion in cleft palate patients is consistently a topic of debate. Formation of a fistula is a risk, and early expansion of the cleft area may lead to more vulnerable bone grafting sites, but these circumstances are manageable by surgeons. The benefits of early expansion include improved stability and eruption of impacted teeth through the alveolar bone. The consequence is that early repair may result in scarring of tissues and make future expansion less favorable. Nevertheless, our craniofacial team prefers to perform early expansion, anticipating opening of the clefts and fistula formation, and we treat these conditions surgically.

Patients with UCLP often have an anterior crossbite that needs to be corrected for functional and esthetic reasons. An anatomically accurate model of the cranio-facial complex allows for precise determination of the force distribution from externally applied forces. This study is novel because it is the first to evaluate the effects of RPE in patients with UCLP in an attempt to improve the quality of their care. RPE is an effective treatment modality for the correction of transverse discrepancies and protraction of the maxilla[16] and is commonly used as part of the sequential treatment for patients with CLP.[5–8] This study is unique because 9 simulated mechanics were used to analyze the stress distributions within the craniofacial complex of a patient with UCLP based on the directions of the forces to obtain optimal palatal expansion.

The FEM is a well-proven and efficient mathematic instrument for evaluating orthodontic concerns and analyzing the effects of expansion devices on the cranio-facial complex in a noninvasive manner.[12,17–19] With finite element analysis, the point of application, magnitude, and direction of a force can be adjusted to simulate clinical situations, and the amount of stress experienced at any point can be theoretically measured.[18,20] Comparisons of the stress levels of internal structures between the cleft and noncleft sides can then be

made so that optimal points of force application for maximum anterolateral expansion of the minor segment can be predicted.

Over the past years, simulation models of the facial model have improved in geometric precision.[12] The FEM of the skull in a study by Iseri et al[18] in 1998 consisted of 2349 individual elements, and an increase in the geometric precision was observed in a 2003 study by Jafari et al[19] that introduced a model with 6951 elements. In 2007, Holberg et al[12] used a simulation model of the facial skull and cranial base that consisted of approximately 30,000 elements and 50,000 nodes. The FEM of the craniofacial complex introduced here consisted of 371,605 elements and 105,357 nodes to create an accurate 3D model. Despite this complex geometric illustration of the skull, our study represents 1 subject's anatomy, and the results about transverse expansion of the maxilla should be interpreted accordingly.

In all 9 simulated palatal expansion cases, the body of the sphenoid had the highest stress concentration because of palatal expansion. The body of the sphenoid experiences high stress levels because it is bent laterally during palatal expansion; as an unpaired bone, it cannot be separated in a similar fashion as the paired maxillary bones.[21–23] Our findings agree with previous studies that have shown that transverse expansion forces generated during RPE are transmitted via the pterygomaxillary connection to the sphenoid of the cranial base.[21–23] Furthermore, the peak first principal stress levels on the body of the sphenoid averaged 1.5 times greater on the cleft side than on the noncleft side.

Stress distribution between the cleft and noncleft sides is asymmetric because of differences in the masses and support structures of the minor and major segments of the maxilla. Lee et al[20] demonstrated in normal patients that the superior and posterior maxillary regions are the final stress-bearing areas after midpalatal suture opening caused by transverse expansion forces. Similarly, in this study, high stress levels at the maxillary buttresses, frontonasal suture, and body of the sphenoid were associated with strong resistance to palatal expansion.

A previous study used the FEM to evaluate the stress pattern in the craniofacial skeleton of a patient with UCLP using surgically assisted rapid maxillary expansion.[13] Researchers found that a more invasive surgically assisted rapid maxillary expansion technique, such as unilateral LeFort I with a midpalatal suture split, can significantly reduce the resultant stresses, but this benefit should be weighed against the risk of increasing complications associated with extensive surgeries.[13] The areas resisting expansion were the infraorbital region and the zygomatic buttress of the noncleft side, followed by the zygomatic buttress of the cleft side; this is consistent with our findings.[13]

Studies that have used transpalatal surgical distraction for maxillary expansion in patients with UCLP have indicated that the vector of distraction should ideally be slightly oblique rather than perpendicular to the midline palatal suture, similar to maxillary constriction in noncleft patients, permitting greater expansion of the more collapsed anterior segment of the maxilla.[24] We also observed the effects of asymmetric transverse expansion forces from RPE in a patient with UCLP and agree that expansion forces applied to the anterior region of the minor segment achieve greater expansion of this segment with minimal expansion of the major segment.

RPE not only affects the dentition and palate but also places stress and strain on various structures in the craniofacial complex, such as the orbits, the pterygoid plates, the body of the sphenoid, and the cranial base. Moderate and high stress concentrations near the medial wall of the orbit on the cleft side, the lateral walls and floors of the orbit, the frontonasal suture, and the sphenoid correlate with clinical presentations of patients feeling heavy pressure at the bridge of the nose, under the eyes, and generally throughout the face. The neurovascular bundles are compressed in these areas, leading to pressure and discomfort for patients undergoing palatal expansion. There is a high risk of relapse of the minor segment after expansion because the stress concentration on the cleft side as a result of palatal expansion is greater than on the noncleft side. Hence, longer retention periods are recommended to allow remodeling of the alveolar and basal bones so that they can withstand stress and prevent orthopedic relapse.

The results from this FEM study show that patients with medial collapse of the minor segment resulting in anterior crossbite without posterior crossbite should have the expansion forces applied to the anterior region of the minor segment and the posterior region of the major segment. If moderate expansion of the posterior segment is needed with anterolateral expansion of the minor segment, expansion forces should be applied to the anterior region of the minor segment and the midsection of the major segment. If the patient has both anterior and posterior crossbites, expansion forces should be applied to the posterior regions of both the major and minor segments.

CONCLUSIONS

1. In patients with UCLP, the stress distribution as a result of transverse expansion forces is asymmetric.

2. Stresses from forces applied to the maxillary teeth are distributed along the trajectories of the 3 maxillary buttresses: nasomaxillary, zygomaticomaxillary, and pterygomaxillary. The first principal stresses at the body of the sphenoid bone on the cleft side are generally 1.5 times greater than those on the normal side. The third principal stresses at the body of the sphenoid bone on the cleft side are generally 2 times greater than those on the normal side.

3. Greater expansion of the minor segment with minimal expansion of the major segment is achieved when expansion forces are applied to the anterior region of the minor segment and the posterior region of the major segment in a patient with UCLP. If there are anterior and posterior crossbites, the expansion forces should be applied to the posterior regions of both the major and minor segments.

Acknowledgments

References

1. Tolarová MM, Cervenka J. Classification and birth prevalence of orofacial clefts. Am J Med Genet. 1998; 75:126–37. [PubMed: 9450872]

2. Bath-Balogh, M., Fehrenbach, MJ. Dental embryology, histology, and anatomy. Philadelphia: Saunders; 1997.

3. Subtelny JD, Brodie AG. An analysis of orthodontic expansion in unilateral cleft lip and cleft palate patients. Am J Orthod. 1954; 40:686–97.

4. Kuroe K, Iino S, Shomura K, Okubo A, Sugihara K, Ito G. Unilateral advancement of the maxillary minor segment by distraction osteogenesis in patients with repaired unilateral cleft lip and palate: report of two cases. Cleft Palate Craniofac J. 2003; 40:317–24. [PubMed: 12733963]

5. Pan X, Qian Y, Yu J, Wang D, Tang Y, Shen G. Biomechanical effects of rapid palatal expansion on the craniofacial skeleton with cleft palate: a three-dimensional finite element analysis. Cleft Palate Craniofac J. 2007; 44:149–54. [PubMed: 17328641]

6. Matthews D. Rapid expansion in clefts. Plast Reconstr Surg. 1975; 56:396–401. [PubMed: 1099589]

7. Lypka M, Yen S, Urata M, Hammoudeh J. Solving convergent vector problems with internal maxillary distractors through the use of a fixed rapid palatal expander. J Oral Maxillofac Surg. 2012; 70:e428–30. [PubMed: 22698298]

8. Yang CJ, Pan XG, Qian YF, Wang GM. Impact of rapid maxillary expansion in unilateral cleft lip and palate patients after secondary alveolar bone grafting: review and case report. Oral Surg Oral Med Oral Pathol Oral Radiol. 2012; 114:e25–30.

9. Thompson JR. The cleft lip and palate problem. Angle Orthod. 1952; 22:137–41.

10. Mark WJ. Development of the face and palate. Cleft Palate Craniofac J. 1995; 32:522–4.

11. Capelozza Filho L, De Almeida AM, Ursi WJ. Rapid maxillary expansion in cleft lip and palate patients. J Clin Orthod. 1994; 28:34–9. [PubMed: 8040239]

12. Holberg C, Holberg N, Schwenzer K, Wichelhaus A, Rudzki-Janson I. Biomechanical analysis of maxillary expansion in CLP patients. Angle Orthod. 2007; 77:280–7. [PubMed: 17319763]

13. Gautam P, Zhao L, Patel P. Biomechanical response of the maxillofacial skeleton to transpalatal orthopedic force in a unilateral palatal cleft. Angle Orthod. 2011; 81:503–9. [PubMed: 21299384]

14. Chaconas SJ, Caputo AA. Observation of orthopedic force distribution produced by maxillary orthodontic appliances. Am J Orthod. 1982; 82:492–501. [PubMed: 6760725]

15. Ghasemianpour M, Ehsani S, Tahmasbi S, Bayat M, Ghorbanpour M, Safavi SM, et al. Distraction osteogenesis for cleft palate closure: a finite element analysis. Dent Res J. 2014; 11:92–9.

16. Scolozzi P, Verdeja R, Herzog G, Jaques B. Maxillary expansion using transpalatal distraction in patients with unilateral cleft lip and palate. Plast Reconstr Surg. 2007; 119:2200–5. [PubMed: 17519722]

17. Tanne K, Hiraga J, Kakiuchi K, Yamagata Y, Sakuda M. Biomechanical effect of anteriorly directed extraoral forces on the cranio-facial complex: a study using the finite element method. Am J Orthod Dentofacial Orthop. 1989; 95:200–7. [PubMed: 2923100]

18. I eri H, Tekkaya AE, Oztan O, Bilgiç S. Biomechanical effects of rapid maxillary expansion on the craniofacial skeleton, studied by the finite element method. Eur J Orthod. 1998; 20:347–56. [PubMed: 9753816]

19. Jafari A, Shetty KS, Kumar M. Study of stress distribution and displacement of various craniofacial structures following application of transverse orthopedic forces—a three-dimensional FEM study. Angle Orthod. 2003; 73:12–20. [PubMed: 12607850]

20. Lee H, Ting K, Nelson M, Sun N, Sung SJ. Maxillary expansion in customized finite element method models. Am J Orthod Dentofacial Orthop. 2009; 136:367–74. [PubMed: 19732671]

21. Snow, JB., Wackym, PA. Ballenger's otorhinolaryngology: head and neck surgery. Beijing, China: People's Medical Publishing House; 2009.

22. Timms DJ. A study of basal movement with rapid maxillary expansion. Am J Orthod. 1980; 77:500–7. [PubMed: 6989258]

23. Holberg C. Effects of rapid maxillary expansion on the cranial base—an FEM-analysis. J Orofac Orthop. 2005; 66:54–66. [PubMed: 15711900]

24. Korioth TW, Versluis A. Modeling the mechanical behavior of the jaws and their related structures by finite element (FE) analysis. Crit Rev Oral Biol Med. 1997; 8:90–104. [PubMed: 9063627]
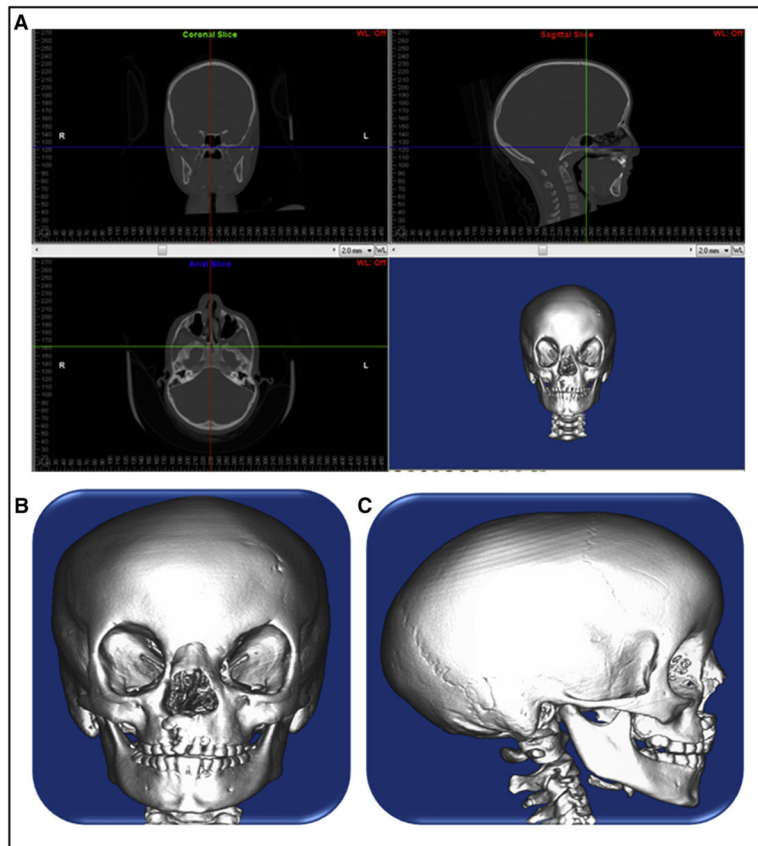
Fig 1.
A, Multiplanar view of the CT data; **B,** 3D solid rendering of the skull of a patient with UCLP using spiral CT data; **C,** lateral view of the 3D solid rendering of the skull a patient with UCLP using spiral CT data.
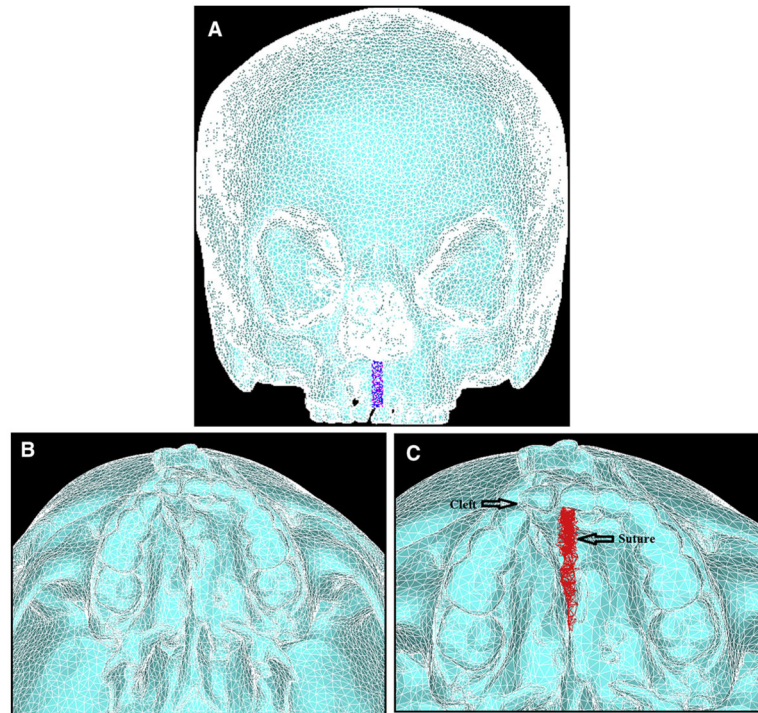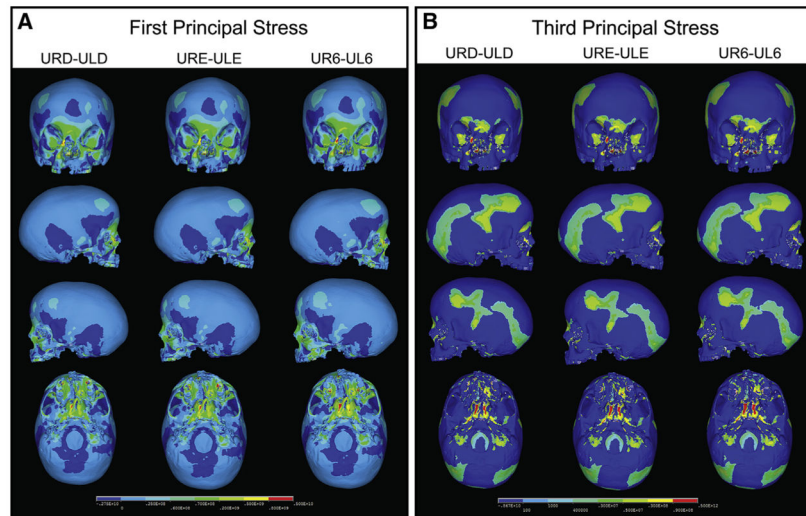
Fig 2.
A, FEM generated from the 3D solid model; **B,** occlusal view of the maxilla with unilateral cleft palate; **C,** occlusal view of the maxilla with unilateral cleft palate and midpalatal suture.
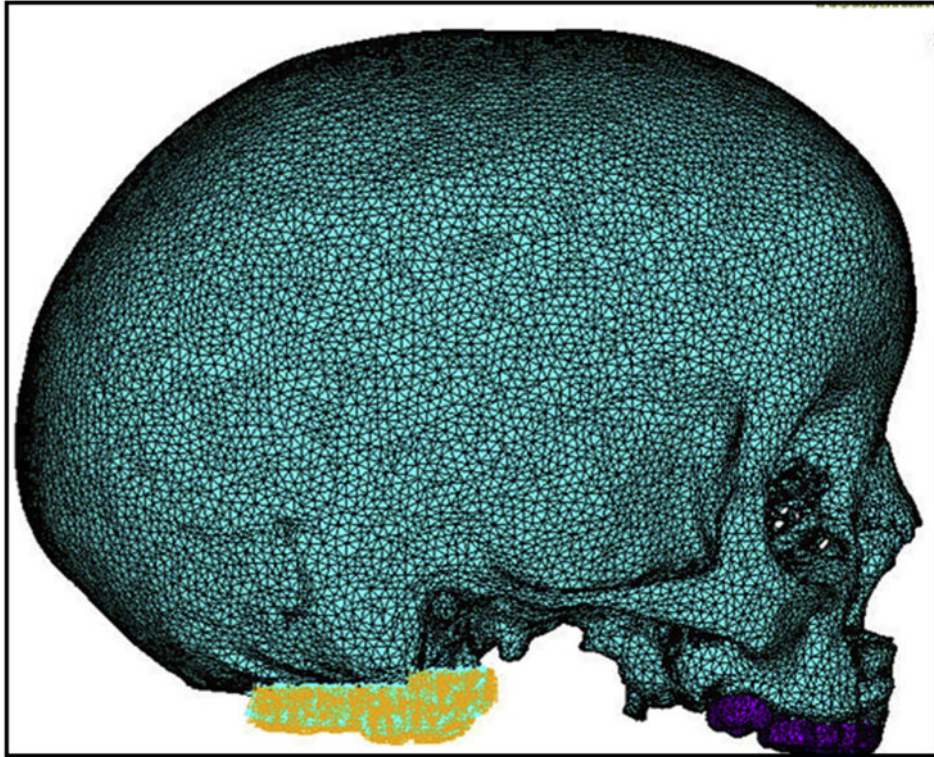
Fig 3.
Lateral view of FEM with constraints on the nodes along the foramen magnum.
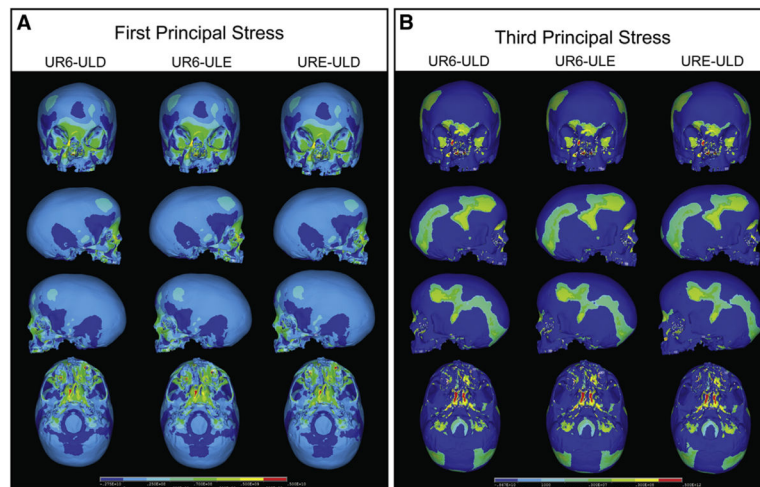
Fig 4.
A, First principal stress distribution of group 1 resulting from expansion forces applied transversely between URD-ULD, URE-ULE, and UR6-UL6; **B,** third principal stress distribution of group 1 resulting from expansion forces applied transversely between URD-ULD, URE-ULE, and UR6-UL6.
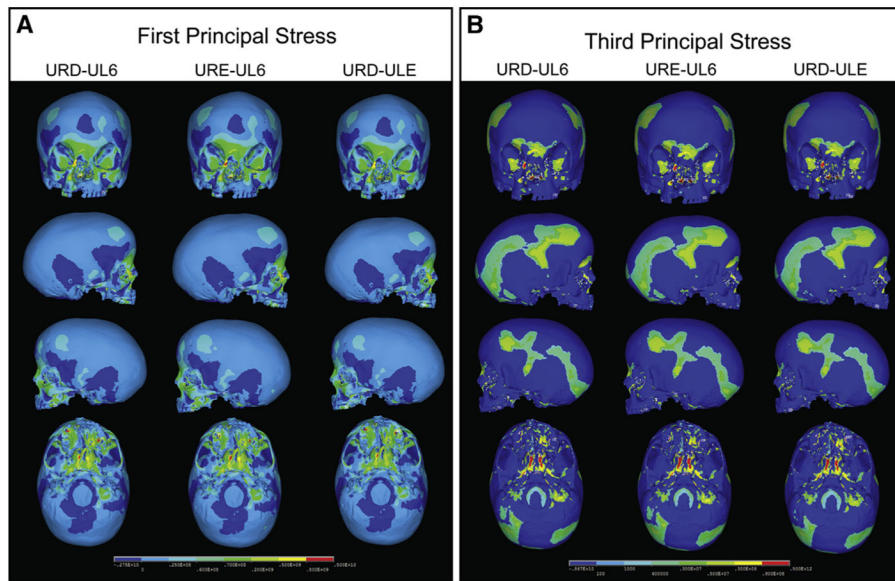
Fig 5.
A, First principal stress distribution of group 2 resulting from expansion forces applied transversely between URD-UL6, URE-UL6, and URD-ULE; **B,** third principal stress distribution of group 2 resulting from expansion forces applied transversely between URD-UL6, URE-UL6, and URD-ULE.

Fig 6.
A, First principal stress distribution of group 3 resulting from expansion forces applied transversely between UR6-ULD, UR6-ULE, and URE-ULD; **B,** third principal stress distribution of group 3 resulting from expansion forces applied transversely between UR6-ULD, UR6-ULE, and URE-ULD.
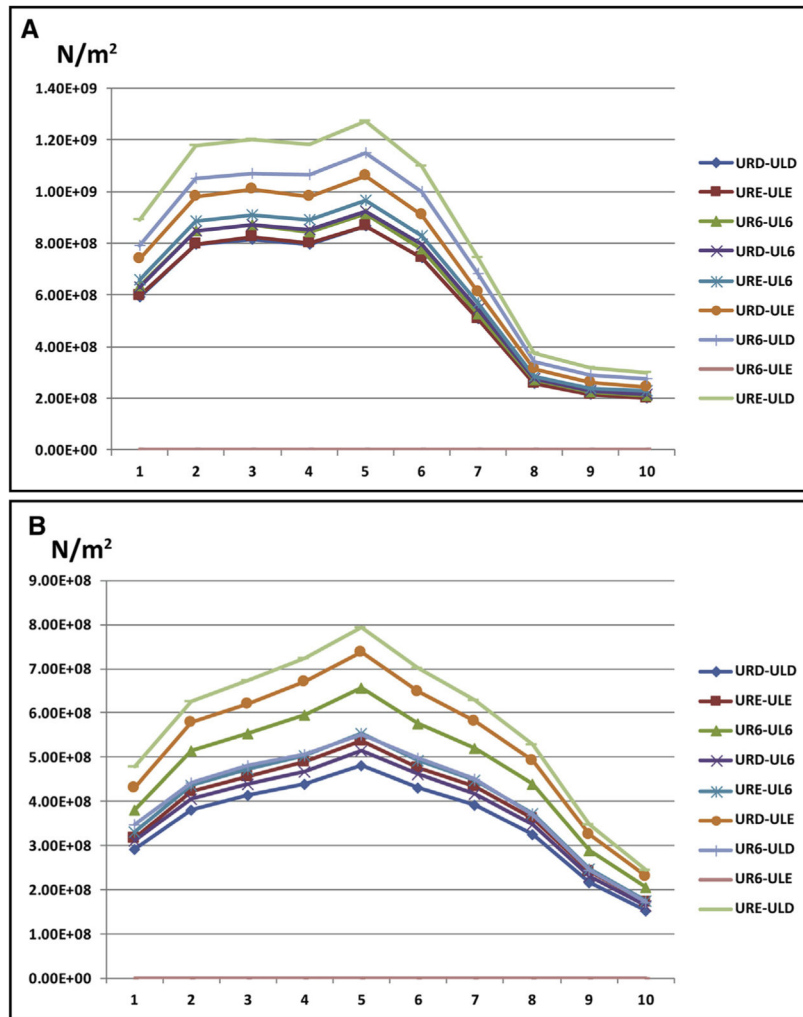
Fig 7.
A, First principal stress from the anterior to the posterior body of the sphenoid on the cleft side; **B,** first principal stress from the anterior to the posterior body of the sphenoid on the normal side.
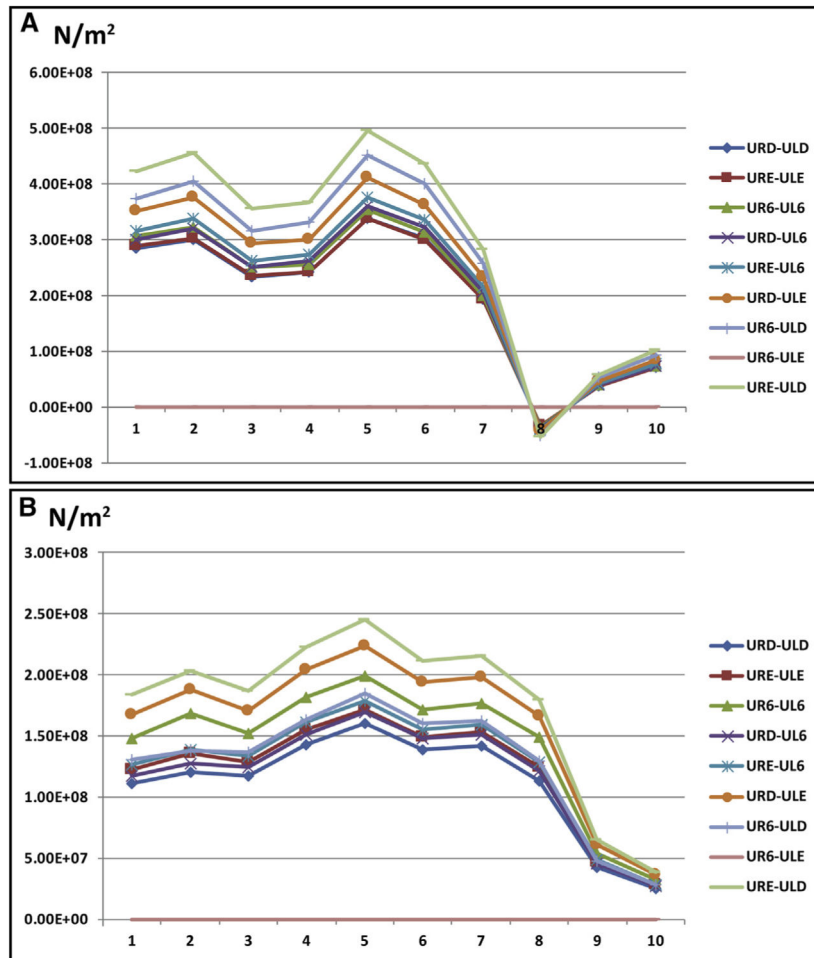
Fig 8.
A, Third principal stress from the anterior to the posterior body of the sphenoid on the cleft side; **B,** third principal stress from the anterior to the posterior body of the sphenoid on the normal side.

Table I

Material properties of cortical bone, enamel, and suture

	Modulus of elasticity, E (GPa)	Poisson coefficient, ν
Cortical bone	13.4	0.3
Enamel	20.2	0.3
Suture	0.08	0.49

Table II

Nine simulated combinations to test maxillary expansion with deciduous molars, permanent molars, or a combination of the molars as anchors

Expansion force applied to teeth	Abbreviations
Maxillary right deciduous first molar to maxillary left deciduous first molar	URD-ULD
Maxillary right deciduous second molar to maxillary left deciduous second molar	URE-ULE
Maxillary right permanent first molar to maxillary left permanent first molar	UR6-UL6
Maxillary right deciduous first molar to maxillary left deciduous second molar	URD-ULE
Maxillary right deciduous first molar to maxillary left permanent molar	URD-UL6
Maxillary right deciduous second molar to maxillary left deciduous first molar	URE-ULD
Maxillary right deciduous second molar to maxillary left permanent first molar	URE-UL6
Maxillary right permanent molar to maxillary left deciduous first molar	UR6-ULD
Maxillary right permanent first molar to maxillary left deciduous second molar	UR6-ULE